Low-Voltage Ride-Through Operation of Power Converters in Grid-Interactive Microgrids by Using Negative-Sequence Droop Control

Zhao, Xin; Guerrero, Josep M.; Savaghebi, Mehdi; Quintero, Juan Carlos Vasquez; Wu, Xiaohua; Sun, Kai

Published in:
I E E E Transactions on Power Electronics

DOI (link to publication from Publisher):
10.1109/TPEL.2016.2570204

Publication date:
2017

Document Version
Early version, also known as pre-print

Low-Voltage Ride-Through Operation of Power Converters in Grid-Interactive Microgrids by Using Negative-Sequence Droop Control

Xin Zhao, *Student Member*, *IEEE*, Josep M. Guerrero, *Fellow*, *IEEE*, Mehdi Savaghebi, *Senior Member*, *IEEE*, Juan C. Vasquez, *Senior Member*, *IEEE*, Xiaohua Wu, Kai Sun, *Senior Member*, *IEEE*

***Abstract*—Due to the increasing penetration level of microgrids (MGs), it becomes a critical issue for MGs to help sustaining power system stability. Therefore, ancillary services, such as the low-voltage ride-through (LVRT) capability should be incorporated in MGs in order to guarantee stable operation of the utility grid during grid faults. In this paper, a LVRT control strategy based on positive/negative sequence droop control is proposed for grid-interactive MGs to ride-through voltage sags with not only inductive/resistive, but also complex line impedance. By using the proposed control strategy, MGs can support the grid voltage, make profits, and also ride-through the voltage dip during the whole fault period. A two layer hierarchical control strategy is proposed in this paper. The primary controller consists of voltage and current inner loops, a conventional droop control and a virtual impedance loop, while the secondary controller is based on a positive/negative sequence droop scheme which is able to coordinate the power injection during voltage sags. Experimental results are obtained to verify the effectiveness of the proposed control strategy.**

***Index Terms*—Grid-interactive microgrid, hierarchical control, low-voltage ride-through, negative sequence droop control.**

I. Introduction

DRIVEN by the economic, political, and environmental issues, renewable energy sources (RESs), such as wind turbines (WT) and photovoltaic (PV) arrays, combined with energy storage systems (ESSs), such as batteries, super-capacitors and flywheels, are integrated into the future distribution networks such as microgrids (MGs) [1], as shown in Fig. 1.

Manuscript received October 15, 2015; revised December 22, 2015; accepted May 11, 2016. This work was supported by the Danish Energy Technology Development and Demonstration Program (EUDP) through the Sino-Danish Project "Microgrid Technology Research and Demonstration" (meter.et.aau.dk), and by the International Science & Technology Cooperation Program of China, project Number: 2014DFG62610.

X. Zhao, J. M. Guerrero, M. Savaghebi, and J. C. Vasquez are with the Department of Energy Technology, Aalborg University, Aalborg 9220, Denmark (e-mail: xzh@et.aau.dk; joz@et.aau.dk; mes@et.aau.dk; juq@et.aau.dk).

X. Wu is with the Key Laboratory of Power Electronics for Energy Conservation and Motor Drive, Department of Electrical Engineering, Northwestern Polytechnical University, Xi'an 710072, China (e-mail: wxh@nwpu.edu.cn).

K. Sun is with the State Key Laboratory of Power Systems, Tsinghua University, Beijing 100084, China (e-mail: sun-kai@mail.tsinghua.edu.cn).

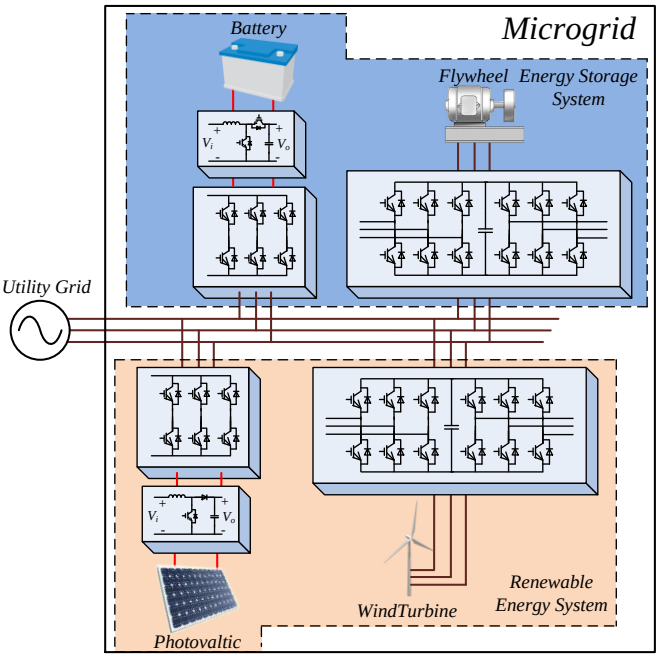

Fig. 1. General structure of a grid-interactive microgrid.

Thanks to advanced power electronic systems, MGs can not only energize the local loads, but also deliver electricity with high reliability and quality to the grid. However, due to the continuously increasing capacity of grid-interactive MGs, these small scale power systems now play a more crucial role than ever before concerning low-voltage ride-through (LVRT) capability. Unfortunately, most of the existing LVRT control strategies [2]−[6] mainly focused on wind farms or large PV plants, meanwhile the current LVRT practice of MGs is simply disconnect them from the grid once faults are detected [7], [8]. This practice suffers from several drawbacks. The first is that this passive strategy will not be an economical option, since the MGs operate in islanded mode during the faults. As a consequence, power generated in the MGs may be wasted, if, for instance, ESSs are fully charged. The second is that the abnormal voltage caused by disconnecting MG with the grid [9] may lead to potential damage to the electrical equipment which is not desired in both safety and power quality point of view. The third drawback of isolating the MGs is that a reconnection process, which may lead to excessive inrush current [10], is required after the fault is cleared. Thus, to help MGs smoothly

over the faults without losing profits and to enhance power system reliability, a LVRT control strategy is proposed in this paper to aid the MGs not only ride-through the grid faults, but also support the grid voltage, generate profits, and eliminate the voltage abnormality during the whole fault period.

Conventionally, LVRT in PV plants is achieved by means of controlling output current of the grid-interactive converter which phase is synchronized with the grid by using phase-locked-loop (PLL), meanwhile a current loop ensures power injection accuracy and current quality issues [11], [12]. In [11], a reactive current injection (RCI) strategy is proposed for single-phase grid-connected PV inverter. In this case, the reactive current reference is set according to the grid code while the active current is limited by considering the converter capacity. LVRT of a three-phase PV converter has been discussed in [13], due to the presence of asymmetrical grid faults, negative sequence current is also injected to suppress the negative sequence voltage. Besides, LVRT in wind farms usually has the objective of injecting balanced three-phase currents or nullifying the 100Hz power oscillations by controlling the grid side converter (GSC) [13]−[15]. In [14], a LVRT control strategy, which is the synthesis of demagnetization and virtual resistance control, is proposed to eliminate the disturbance of stator flux and limit the stator side current. A flexible voltage support strategy is proposed in [6], which can equip the converters with the capability of positive sequence voltage recovery and negative sequence voltage suppression. Later, a LVRT strategy, which has a similar objective as that in [6], is illustrated in [16] by taking the network impedance impact into account. However, all the aforementioned control strategies are proposed for converters operating in current-controlled mode, while the LVRT capability for the widely used droop-controlled converters [11], [17]−[18] in MGs is barely studied.

Moreover, the aim of this paper is to provide a LVRT strategy for MGs which has different objectives with the LVRT method utilized in the conventional PV/WT power plant. In MGs, high power quality is usually required at the AC bus to ensure the normal operation of the local electrical loads. This means that it is critical to maintain both voltage and frequency at the AC bus constant. However, in most of the publications [2], [11]−[15], the line impedance, which has a great influence on the amplitude and phase angle of the compensation voltage, is simply deemed as pure inductive (medium/high-voltage grid) or pure resistive (low-voltage grid). Therefore, the AC bus voltage cannot be compensated accurately, and the AC bus power quality cannot be maintained at a satisfied level during voltage sags. In order to address this problem, complex line impedance is considered to control the amplitude and phase angle of the current injected by the converters.

Thus, to embed the voltage-controlled converters with LVRT capability, negative sequence droop control is proposed in this paper to make the MGs not only maintain connected with the utility grid under voltage sags, but also support the grid voltage by injecting positive and negative sequence power with a satisfied power sharing accuracy among the distributed converters.

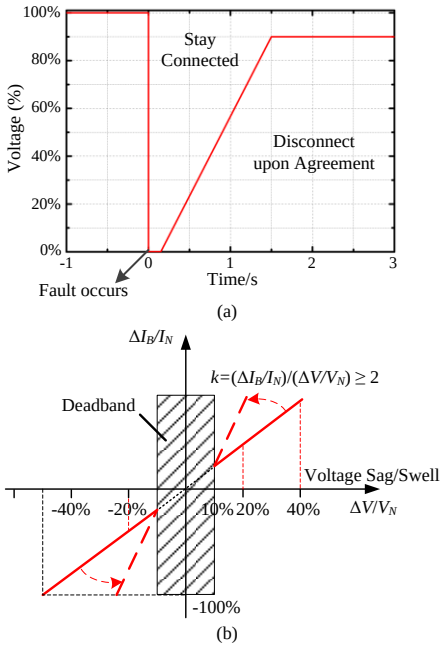

Fig. 2. German grid code requirements. (a) LVRT capability and (b) reactive power support capability.

The rest of the paper is organized as follows. In Section II, a brief introduction to the existing grid code is presented to assist designing of the proposed controller. Section III analyses the voltage and current phasors by using symmetrical component theory. Section IV shows the overall hierarchical control scheme while the proposed LVRT controller is illustrated in Section V. Section VI studies the small signal stability of the proposed negative sequence control system. Section VII provides the simulation and experimental results of a lab-scale MG that consists of two parallel converters connected to the grid. Finally, the conclusions are presented in Section VIII.

II. Grid Code Requirements

Conventionally, the distributed generators (DGs) are required to disconnect from the grid when voltage sags occur and to reconnect to the grid when faults are cleared [7], [8], [19]. However, with the increasing penetration level of the grid-interactive MGs, it is preferred that MG could also maintain active power delivery and provide reactive power support during the period of voltage sag, since it may alleviate the potential instability problems. Thus, many countries have revised their grid codes to accommodate with the increasing capacity of RES. Spain, German and Denmark have already published the LVRT and reactive current injection requirements for grid-connected RESs in 2005, 2007 and 2010, respectively [20]−[22]. As an example, the German E.ON NetZ code is shown in Fig. 2 [21]. Although this requirement is designed for high voltage grid, it is applicable to low-voltage grid since they have similar concepts.

It can be seen in Fig. 2(a) that only when the grid voltage falls below the red curve, DGs are allowed to disconnect with the grid. Otherwise, DGs should inject a certain amount of reactive power which is defined in Fig. 2(b). As shown in Fig. 2(b), when the grid voltage is lower than $0.9V_N$, 1% drop of the

grid voltage requires at least *k*% increase of the injected current. If needed, it should be capable of supplying 1 p.u. of reactive current. The corresponding equations are given as follows.

$$I_{ref}=\begin{cases}0, & V_g>0.9V_N\\ \left(-k\cdot\dfrac{V_g}{V_N}+k\right)\cdot I_N, & 0.9V_N\ge V_g>0.5V_N,\quad k\ge 2\\ I_N, & V_g\le 0.5V_N\end{cases}\quad(1)$$

where V_N is the nominal grid voltage, I_N is the converter rated current, ΔV is the depth of voltage sag, and ΔI_B is the increment of reactive current after fault occurs. Note that the constant k should be no less than 2 p.u. according to the German grid code [21].

III. Voltage and Current Phasor Analysis based on Symmetrical Components Decomposition

According to the symmetrical sequence theory [23], the instantaneous voltage/current can be represented by positive sequence, negative sequence and zero sequence components.

$$\begin{bmatrix}x_a\\x_b\\x_c\end{bmatrix}=\begin{bmatrix}x_a^+\\x_b^+\\x_c^+\end{bmatrix}+\begin{bmatrix}x_a^-\\x_b^-\\x_c^-\end{bmatrix}+\begin{bmatrix}x_a^0\\x_b^0\\x_c^0\end{bmatrix}\quad(2)$$

where x_a, x_b, and x_c represent the *abc* component of voltage or current phasors, and superscript "+", "–" and "0" denote the positive, negative and zero sequence, respectively. Zero sequence components are neglected, since the MG is considered three-phase three-wire in this paper.

Based on (2), the instantaneous active and reactive power can be expressed as

$$p=P^+ +P^- +p_{2\omega}=v^+i^+ +v^-i^- +(v^+i^- +v^-i^+)\quad(3)$$

$$q=Q^+ +Q^- +q_{2\omega}=v_\perp^+i^+ +v_\perp^-i^- +(v_\perp^+i^- +v_\perp^-i^+)\quad(4)$$

$$v^{+/-}=\begin{bmatrix}v_\alpha^{+/-} & v_\beta^{+/-}\end{bmatrix}\quad(5)$$

$$v_\perp^{+/-}=\begin{bmatrix}v_\beta^{+/-} & -v_\alpha^{+/-}\end{bmatrix}\quad(6)$$

$$i^{+/-}=\begin{bmatrix}i_\alpha^{+/-} & i_\beta^{+/-}\end{bmatrix}^T\quad(7)$$

where $P^{+/-}$ and $Q^{+/-}$ are positive and negative sequence active and reactive power, $p_{2\omega}$ and $q_{2\omega}$ are oscillation terms of active and reactive power, $v^{+/-}$ and $i^{+/-}$ represent for the positive and negative sequence components of voltage and current, respectively, and $\perp$ denotes the corresponding orthogonal vector.

From (3) to (7), it can be seen that the active and reactive power in positive and negative sequence are independent from each other. Consequently, different control strategies can be designed to separately control the positive and negative sequence power regarding different applications, e.g., maximum positive sequence voltage restoration, maximum voltage unbalance mitigation, and so forth. Note that the presence of oscillating power ($p_{2\omega}$ and $q_{2\omega}$) is due to the interaction between voltage and current in different sequences.

The power flow between the converter and the grid is shown in Fig. 3. In the figure, v_g and v_c are the grid voltage and converter voltage, respectively. Z_g and Z_o are the grid impedance and the converter closed-loop output impedance, respectively.

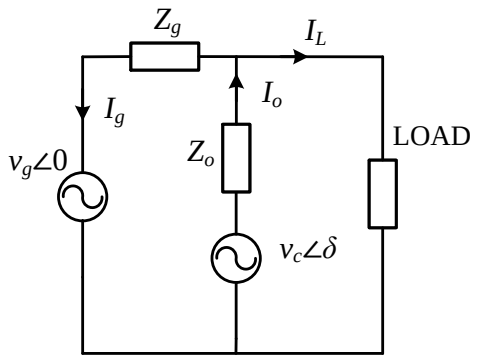

Fig. 3. Power flow diagram between the converter and the grid.

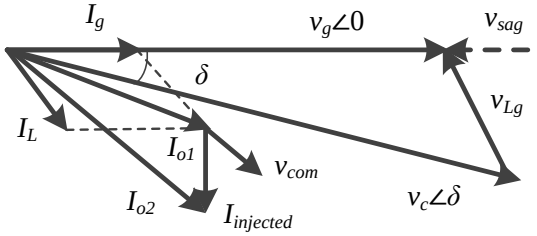

Fig. 4. Steady-state phasor diagram with only reactive current injection under complex line impedance condition.

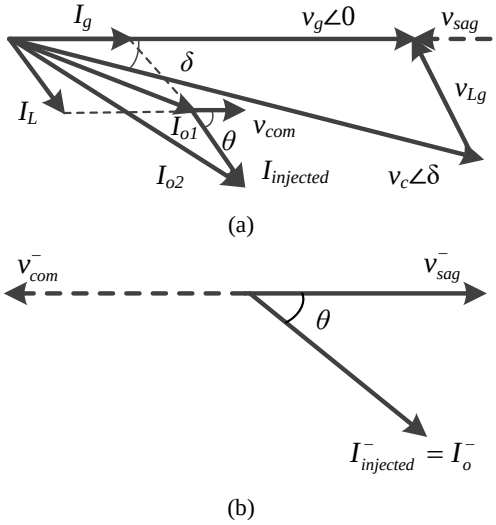

Fig. 5. Steady-state phasor diagram with both active and reactive current injection under complex line impedance condition. (a) positive sequence diagram and (b) negative sequence diagram.

Generally, Z_g and Z_o are considered mainly inductive due to the large output inductor [24]. However, this is not always true, since Z_o also depends on the adopted control strategy [25], while Z_g can be mainly resistive in low-voltage grids [18]. In fact, MGs may locate far from the grid, where non-negligible inductive and resistive line impedance may also present [26]. Due to the aforementioned facts, line impedance is considered complex in this paper. In this case, if only reactive current is injected during the voltage sag, the compensated voltage will not be in phase with v_g, as shown in Fig. 4. In this figure, v_{sag} is the depth of the voltage sag, v_{Lg} is the voltage drop on grid impedance, $I_{injected}$ and v_{com} are the compensation current and

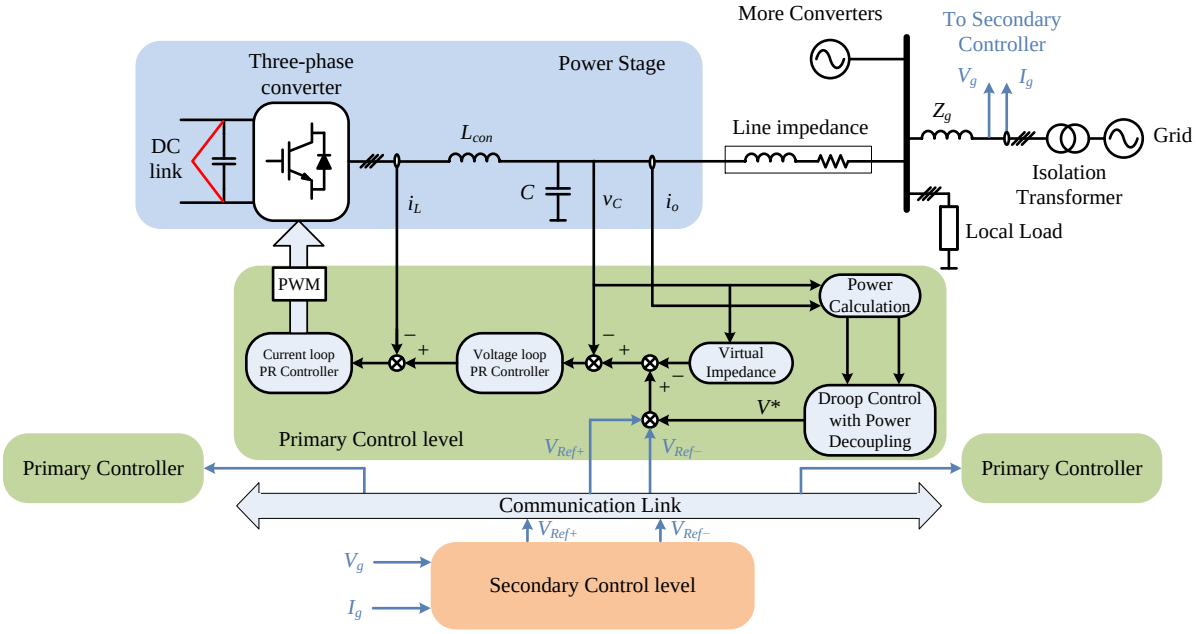

Fig. 6. Hierarchical control scheme.

voltage, respectively, while I_{o1} and I_{o2} are the converter output current before and after the sag, respectively.

Positive and negative sequence phasor diagrams with both active and reactive current injection are illustrated in Fig. 5. Note that θ is the angle of line impedance. In Fig. 5(a), phase angle of the injected current is θ rather than 90°, i.e. the converter should inject not only reactive power, but also active power to support the positive sequence voltage. Meanwhile, Fig. 5(b) shows that the angle between negative sequence voltage and injected current is $180°-\theta$, i.e., the converter should inject negative sequence reactive power and absorb negative sequence active power simultaneously.

Thus, not only positive sequence active/reactive power, but also negative sequence active/reactive power is needed to recover and balance the load side voltage under asymmetrical voltage sags. Therefore, by using the negative/positive sequence droop control, which is proposed in Section V, the converter voltage reference can be modified to control the power injected by the converter.

Based on the abovementioned analysis, the injected current during the voltage sag can be written as

$$I_{o2} = I_L + I_g \tag{8}$$

$$I_g = I_g^+ + I_g^- = \frac{v_{sag}^+}{Z_g} + \frac{v_{sag}^-}{Z_g} \tag{9}$$

where I_g^+ and I_g^- are the injected positive and negative sequence current, respectively, v_{sag}^+ and v_{sag}^- are the positive and negative sequence sag voltage, respectively.

From (8) and (9), it can be seen that during the voltage sag, the amount of positive and negative sequence current needed to restore the positive sequence voltage or eliminate the negative sequence voltage is inversely proportional to the grid impedance Z_g. Thus, an extra inductor is implemented between the MG and the grid to limit the grid current and also to emulate the leakage inductor of the isolation transformer. However, this inductor will also induce extra voltage drop across it which is not preferred in normal conditions. Consequently, its value should be chosen carefully based on voltage and current ratings of the system.

IV. Hierarchical Control Scheme

In this paper, the grid-interactive MG includes several voltage-controlled converters connected to the grid through *LC* filters, as shown in Fig. 6. A hierarchical control algorithm [27], [28] which consists of primary and secondary control is proposed in this paper.

A. Primary control loop

As shown in Fig. 6, the primary controller includes voltage/current inner loop, droop control loop and virtual impedance loop. These three control loops are implemented in two-phase stationary reference frame ($\alpha\beta$) to reduce computational burden.

Both voltage and current controllers are based on proportional+resonant (PR) controllers to provide satisfactory tracking performance for positive and negative sequence sinusoidal signals [29], [30].

PI based droop control [30], [31] is implemented during normal operation mode, since the whole system operates in grid-interactive mode. Note that the active and reactive power is calculated in primary loop and is followed by low pass filters with 5Hz cut-off frequency which can filter out the power ripples.

A virtual impedance loop [28] is implemented to enhance the power sharing accuracy among the distributed converters, and also to make the system more damped without sacrificing system efficiency.

B. Secondary control loop

Secondary control mainly contributes to the positive and negative sequence power injection under voltage sags in terms

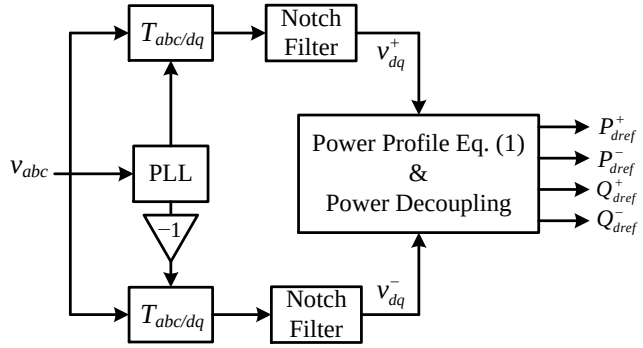

Fig. 7. Power calculation block.

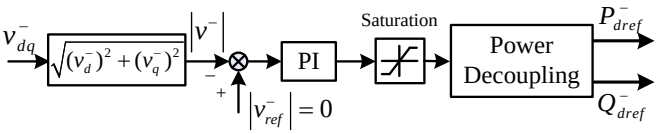

Fig. 8. Negative sequence power reference generation.

of sending voltage sag compensation signals to primary control loop. In this control loop, another power calculation block is used to calculate the positive/negative sequence power by measuring the PCC voltage and current. Then, the calculated powers are afterwards sending to the proposed positive/negative sequence droop controller to generate the positive/negative sequence voltage amplitude and phase signal. Finally, the generated signals are transformed into *αβ* coordinates and added to the voltage loop controller. Detailed design procedure of the proposed controller will be shown in the next section. Considering that the duration of grid faults are usually very short, high bandwidth communication link is needed between primary and secondary controller, and in the experiments it is emulated in *dSPACE* with 10kHz update rate.

The detailed description of the power calculation block is shown in Fig. 7. Two *d-q* transformation blocks followed by notch filters are employed to extract interested sequence components. Then, by utilizing the extracted components, positive/negative sequence power can be obtained. Note that the extracted negative sequence grid voltage also determines whether to activate the secondary controller. Detailed design of the filter can be found in [32]. It is worth mentioning that the negative sequence power reference can be calculated by using the strategy shown in Fig. 8. In such a way the voltage unbalance can be suppressed to a large extent.

V. Proposed LVRT Controller

Once voltage sag occurs, the positive and negative sequence voltage can be deduced as

$$\vec{V}_P = m\vec{V}^+_{Sa} \tag{10}$$

$$\vec{V}_N = n\vec{V}^+_{Sa} \tag{11}$$

where $\vec{V}^+_{Sa}$ represents pre-fault voltage vector of phase A, while *m* and *n* are constants which are related to the type and depth of the voltage sag [33].

As illustrated in [33], along with the drop of positive sequence voltage, negative sequence voltage will also appear. Thus, it is necessary to inject not only positive sequence power,

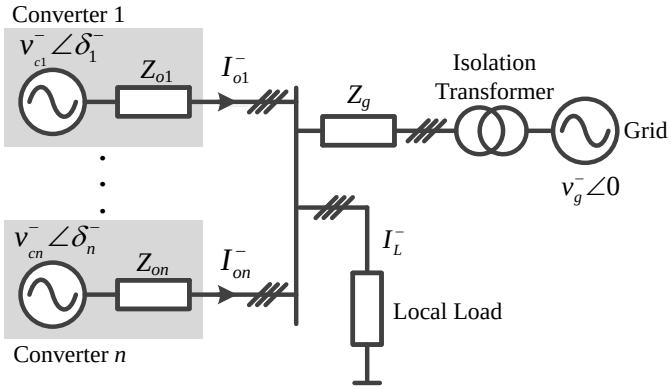

Fig. 9. Negative sequence equivalent circuit.

but also negative sequence power when asymmetrical sag occurs. The design of the positive sequence droop control will not be discussed here, since it is well-addressed in the previous literatures [18], [27]−[29].

In order to control the injected negative sequence power and eliminate the circulating current among the converters, a dedicated negative sequence droop controller is designed in this section, and the equivalent circuit of the studied system is depicted in Fig. 9.

From Fig. 9, the output current I^-_{on} injected by the converter can be given by

$$I^-_{on} = \frac{v^-_{cn}\angle\delta^-_n - v^-_g\angle 0}{Z_g\angle\theta} \tag{12}$$

where v^-_{cn} and δ^-_n are the negative sequence amplitude and phase angle of the n^{th} converter output voltage while v^-_g is the negative sequence amplitude of the grid voltage, θ is the phase angle of the grid impedance. Note that phase angle of common AC bus voltage is taken as the phase reference.

Then, the complex power S^-_n injected by the converter is calculated as

$$S^-_n = v^-_{cn}\cdot(i^-_{on})^* = P^-_n + jQ^-_n \tag{13}$$

Finally, the negative sequence active power P^-_n and reactive power Q^-_n injected by the n^{th} DG converter can be obtained as (14) and (15), respectively.

$$P^-_n = \left(\frac{V^-_{cn}V^-_g}{Z_g}\cos\delta^-_n - \frac{(V^-_g)^2}{Z_g}\right)\cos\theta + \frac{V^-_{cn}V^-_g}{Z_g}\sin\delta^-_n\sin\theta \tag{14}$$

$$Q^-_n = \left(\frac{V^-_{cn}V^-_g}{Z_g}\cos\delta^-_n - \frac{(V^-_g)^2}{Z_g}\right)\sin\theta - \frac{V^-_{cn}V^-_g}{Z_g}\sin\delta^-_n\cos\theta \tag{15}$$

It is clear from (14) and (15) that P^-_n and Q^-_n depend simultaneously on both V^-_{cn} and δ^-_n. For simplifications, P^-_n and Q^-_n can be transformed to variables [29] defined as P^-_d and Q^-_d, which are independent from the magnitude and phase of the grid impedance Z_g. The transform equation is given by

$$P^-_d = P^-_n\sin\theta - Q^-_n\cos\theta \tag{16}$$

$$Q^-_d = P^-_n\cos\theta + Q^-_n\sin\theta \tag{17}$$

By substituting (16) and (17) into (14) and (15), and considering δ^-_n is small enough, the following expressions can be yielded

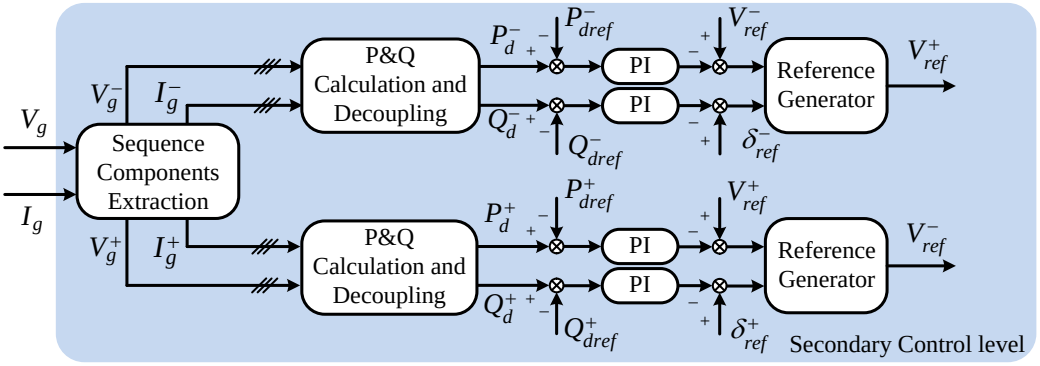

Fig. 10. Proposed LVRT control block based on negative sequence droop method.

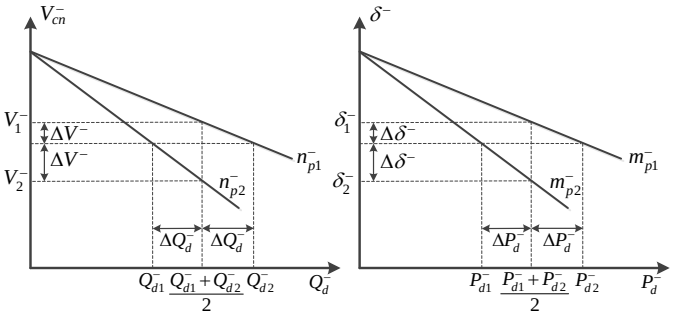

Fig. 11. Steady-state negative sequence droop characteristics.

$$P_d^- \approx \frac{V_{cn}^- V_g^-}{Z_g} \delta_n^- \tag{18}$$

$$Q_d^- \approx \frac{V_{cn}^- V_g^- - (V_g^-)^2}{Z_g} \tag{19}$$

From (18) and (19), it can be concluded that the decoupled power P_d^- and Q_d^- predominately dependent upon the power angle δ_n^- and voltage amplitude V_{cn}^-, respectively, and thus can be implemented in the droop method to control the active and reactive power flow. Consequently, the negative sequence power controller is proposed by introducing artificial droops into negative sequence output voltage reference, i.e., $P_d^- - \delta_n^-$ and $Q_d^- - V_{cn}^-$ droop schemes. The proposed control law is expressed in (20) and (21), and the corresponding block diagram is depicted in Fig. 10.

$$\delta^- = \delta_0^- - (m_p^- + \frac{m_I^-}{s})\left(P_d^- - P_{ref}^-\right) \tag{20}$$

$$V^- = V_0^- - (n_p^- + \frac{n_I^-}{s})\left(Q_d^- - Q_{ref}^-\right) \tag{21}$$

where δ^- and V^- are the amplitude and phase angle of the negative sequence voltage reference, while V_0^- and δ_0^- are the nominal value of the negative sequence voltage amplitude and phase angle, P_{ref}^- and Q_{ref}^- are respectively the reference of fundamental negative sequence active and reactive power, m_p^-, m_I^- and n_p^-, n_I^- are the proportional and integral coefficients for the active and reactive power controllers, respectively. Moreover, it needs to be clarified that since both primary power controller and the proposed LVRT controller changes the voltage reference amplitude and phase angle, thus the primary power controller should be disabled if secondary controller is activated to avoid coupling between these two controllers. Furthermore, if θ is 90 °, the decoupled power will be identical with the real output power of the converters, and thus (20), (21) can still be derived from (14), (15) with the same form expect P_d^- and Q_d^- are replaced by P_n^- and Q_n^-, respectively. These indicate that the proposed control strategy can also function properly under inductive/resistive line impedance.

The steady-state negative sequence droop characteristics are shown in Fig. 11. Obviously, if the proportional droop coefficients m_p^- and n_p^- increase, better power sharing accuracy can be achieved at the expense of degrading the voltage regulation. This inherent tradeoff can be a serious limitation in terms of transient response and power sharing accuracy. In order to fully control the transient behaviors of the converter, the integral coefficients m_I^- and n_I^- are introduced. These two coefficients give us extra freedoms to modify the transient response, meanwhile keeping constant the steady-state frequency and amplitude of the output voltage.

VI. Small Signal Analysis and Control Parameters Design

Small signal model and stability analysis of the proposed negative sequence controller are yielded to show the stability of the system and to properly design the control system parameters.

In order to realize the control strategy defined by (20) and (21), the power injected to the grid should be calculated. And due to the low pass filter used in this calculation, the bandwidth of the inner voltage and current control loops are much higher than that of the outer power control loop. Therefore, the inverter can be assumed as an ideal voltage source which output voltage is directly governed by the references generated by the proposed control law. Then, the small signal dynamics of the filtered negative sequence active and reactive power can be obtained by linearizing (18) and (19).

$$\Delta P_d^- = \frac{\omega_c}{s+\omega_c}\left(\frac{\Delta V_{cn}^- V_g^- \sin\delta^- + \Delta\delta V_g^- V_{cn}^- \cos\delta^-}{Z_g}\right) \tag{22}$$

$$\Delta Q_d^- = \frac{\omega_c}{s+\omega_c}\left(\frac{\Delta V_{cn}^- V_g^- \cos\delta^- - \Delta\delta V_g^- V_{cn}^- \sin\delta^-}{Z_g}\right) \tag{23}$$

where Δ denotes perturbed values while uppercase variables indicates the equilibrium point values, ω_c is the cutoff angular frequency of the low pass filters.

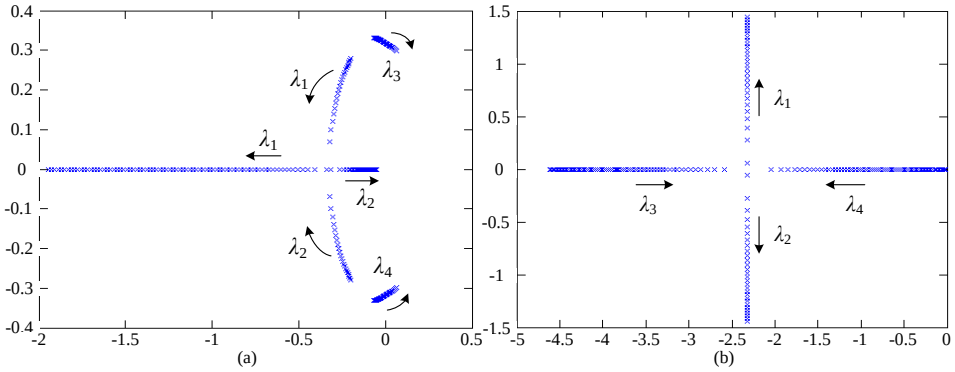

Fig. 12. Root locus diagrams. (a) $0.0001 \le m_p^- \le 0.01$ and (b) $0.0001 \le m_I^- \le 0.01$.

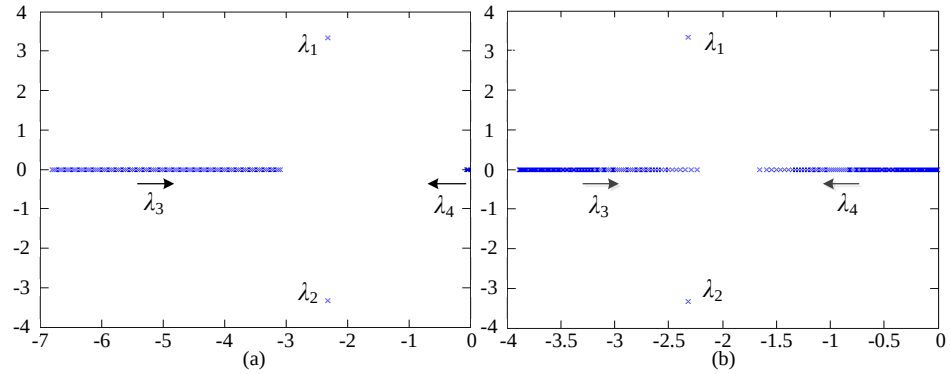

Fig. 13. Root locus diagrams. (a) $0.0001 \le n_p^- \le 0.1$ and (b) $0.0001 \le n_I^- \le 0.1$.

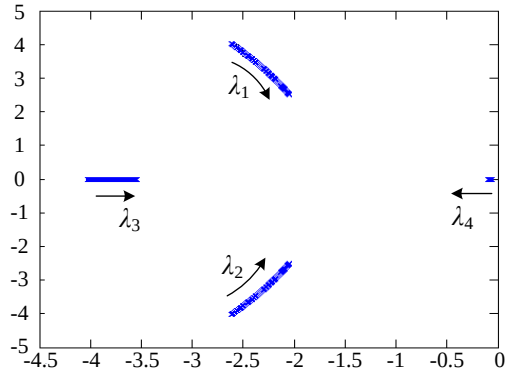

Fig. 14. Root locus diagram when $0.1\text{mH} \le L_g \le 10\text{mH}$.

By linearizing (20) and (21), we have

$$\Delta\delta^- = -(m_p^- + \frac{m_I^-}{s})\Delta P_d^- \tag{24}$$

$$\Delta V_{cn}^- = -(n_p^- + \frac{n_I^-}{s})\Delta Q_d^- \tag{25}$$

Substitute (22), (23) into (24), (25) respectively, we obtain

$$\Delta\delta^- = -(m_p^- + \frac{m_I^-}{s})\frac{\omega_c}{s+\omega_c}\left(k_{pe}\Delta V_{cn}^- + k_{pd}\Delta\delta^-\right) \tag{26}$$

$$\Delta V_{cn}^- = -(n_p^- + \frac{n_I^-}{s})\frac{\omega_c}{s+\omega_c}\left(k_{qe}\Delta V_{cn}^- + k_{qd}\Delta\delta^-\right) \tag{27}$$

where

$$k_{pe} = \frac{V_g^- \sin\delta^-}{Z_g}$$

$$k_{pd} = \frac{V_g^- V_{cn}^- \cos\delta^-}{Z_g}$$

$$k_{qe} = \frac{V_g^- \cos\delta^-}{Z_g}$$

$$k_{qd} = \frac{-V_g^- V_{cn}^- \sin\delta^-}{Z_g}$$

Finally, the small signal dynamics of the closed-loop system can be obtained by substituting (27) into (26)

$$s^4\Delta\delta^- + as^3\Delta\delta^- + bs^2\Delta\delta^- + cs\Delta\delta^- + d\Delta\delta^- = 0 \tag{28}$$

where

$$a = \left(2 + n_p^- k_{qe} + m_p^- k_{pd}\right)\omega_c$$

$$b = \left(1 + n_p^- k_{qe} + m_p^- k_{pd} + m_p^- n_p^- k_{pd} k_{qe} - m_p^- n_p^- k_{pe} k_{qd}\right)\omega_c^2 + \left(m_I^- k_{pd} + n_I^- k_{qe}\right)\omega_c$$

$$c = \left[\left(m_p^- n_I^- + m_I^- n_p^-\right)k_{pd}k_{qe} - \left(m_I^- n_p^- + m_p^- n_I^-\right)k_{pe}k_{qd} + \left(n_I^- k_{qe} + m_I^- k_{pd}\right)\right]\omega_c^2$$

$$d = \left(k_{pd}k_{qe} - k_{pe}k_{qd}\right)m_I^- n_I^- \omega_c^2$$

It is worth noting that the small signal analysis under inductive and resistive line impedance is not presented, since they are merely a special case of complex line impedance. By analyzing (28), the stability of the closed-loop system can be evaluated, and the root locus diagrams are shown in Figs. 12-14 by using the parameters listed in Table I. It can be observed from Fig. 12(a) that faster system dynamic can be obtained by increasing m_p^-. The root locus in Fig. 12(b) shows that by

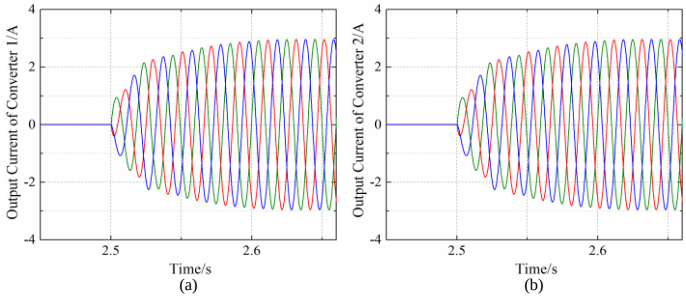

Fig. 15. Output current waveforms of the converters. (a) converter 1 and (b) converter 2.

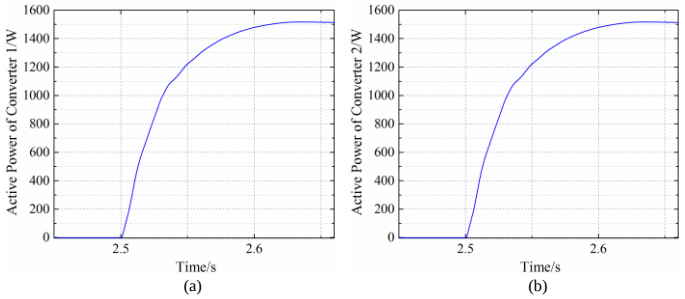

Fig. 16. Active power of the converters. (a) active power and (b) reactive power.

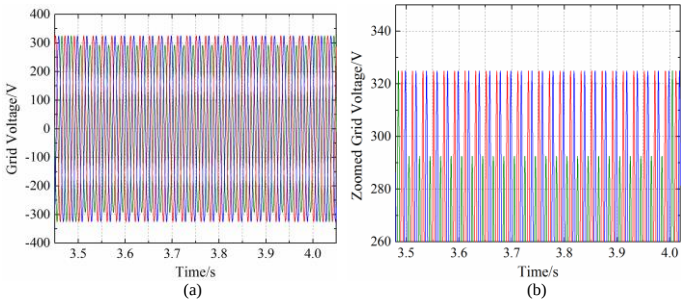

Fig. 17. Grid voltage with 0.1 p.u. voltage sag. (a) grid voltage and (b) zoomed grid voltage.

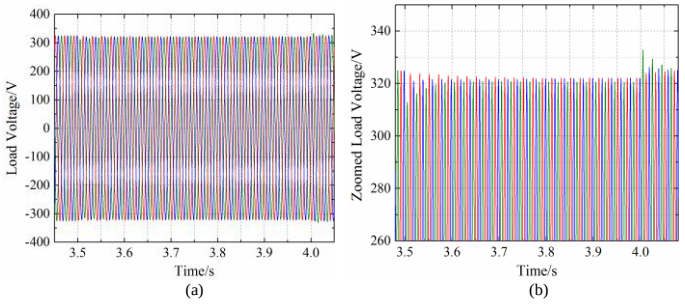

Fig. 18. Load voltage during the sag. (a) load voltage and (b) zoomed load voltage.

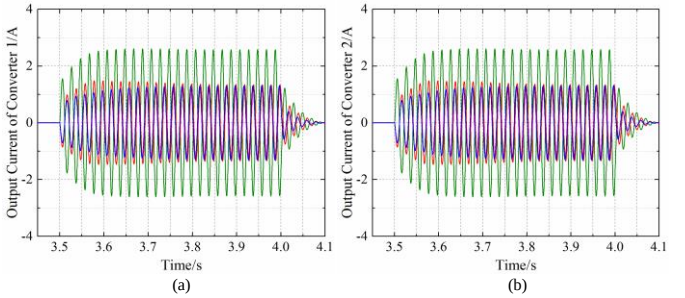

Fig. 19. Output current of the converters. (a) converter 1 and (b) converter 2.

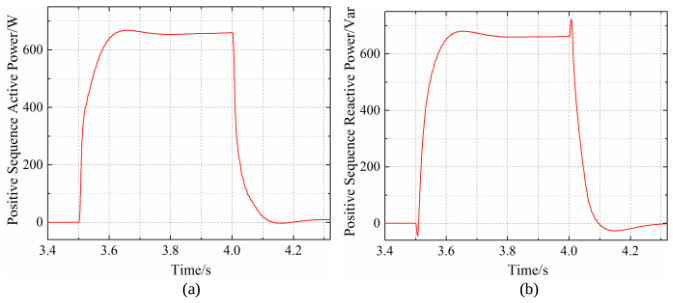

Fig. 20. Positive sequence output power of the converter. (a) active power and (b) reactive power.

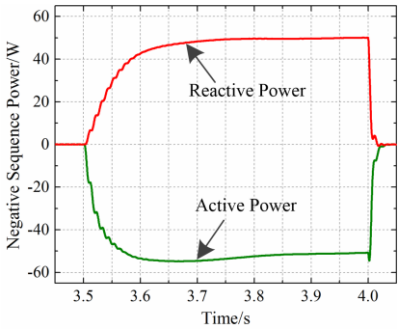

Fig. 21. Negative sequence active power and reactive power.

increasing m_I^-, a near second-order behavior is obtained. Also, the system dynamics by varying n_p^- and n_I^- are shown in Fig. 13. Finally, these four parameters can be selected by locating the poles to where a fast and stable system can be obtained.

The stability of the system has also been evaluated by varying the grid inductance L_g. Fig. 14 shows that the system is stable even if the value of L_g is 0.1 mH. This is because that the grid resistance provides enough damping to the system.

VII. Simulation and Experimental Results

Simulation was conducted for a two-parallel-inverter system connecting to the grid with the configuration shown in Fig.6. Specifications of power stage and control system are given in Table I. Note that per unit value is used in the table, and the base value for power and voltage is 2.2 kVA and 398 V, respectively.

Figs. 15 and 16 show the transient response of the converter output current and active power with the load step from 0 to 1500 W at t = 2.5s. These results show a fast dynamic response of the proposed controller for load step changes, also the equal current sharing is validated.

Simulation has been tested also in the presence of a 0.1 p.u. voltage sag, which occurs at t = 3.5s (shown in Fig. 17). Fig. 18 depicts three-phase load voltage during the voltage sag. It is obvious that the load voltage increased to 320V while the negative sequence voltage becomes almost negligible.

Fig. 19 shows the converter output current. As it can be seen, the current can be shared equally between the converters. The positive/negative sequence active and reactive powers injected to the grid are shown in Fig. 20 and Fig. 21, respectively. It can be seen that the converter can provide appropriate positive and negative sequence power according to the depth of the voltage sag.

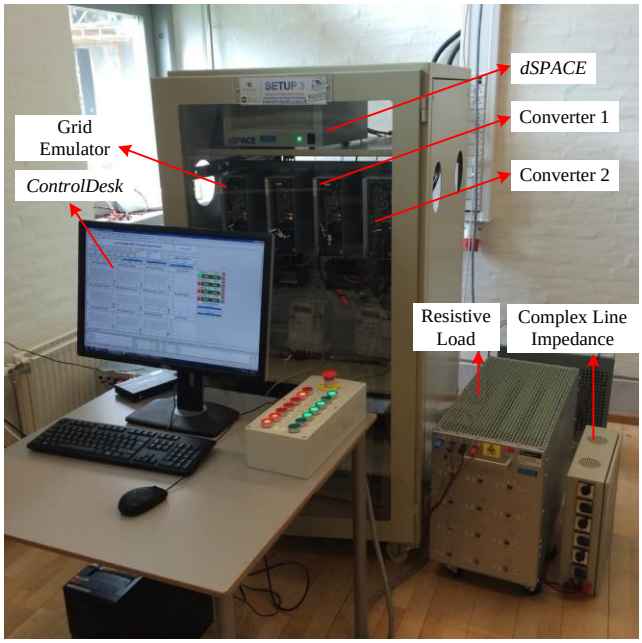

Fig. 22. Experimental testbed.

TABLE I
SYSTEM PARAMETERS

Power Stage Parameters		
Parameters	***Symbol***	***Value***
Converter Side Inductors	L_{con}^*	0.008 p.u.
Grid Side Inductors	L_g^*	0.008 p.u.
Capacitors	C^*	4.9 p.u.
Load	R^*	1 p.u.
Grid Impedance	Z_g^*	0.028+j0.028 p.u.
Nominal Voltage	V^*	1 p.u.
DC Voltage	V_{DC}^*	1.63 p.u.
Nominal Frequency	f	50 *Hz*
Switching Frequency	f_s	10 *kHz*
Primary Controller		
Parameters	***Symbol***	***Value***
Voltage Loop Controller	k_{vp}, k_{vr}	*0.05, 10*
Current Loop Controller	k_{ip}, k_{ir}	*10, 600*
Proportional Phase Droop	m_P	*0.00005*
Integral Phase Droop	m_I	*0.001*
Proportional Voltage Droop	n_P	0.005
Integral Voltage Droop	n_I	0.01
Virtual Impedance	Z_v^*	0.014+j0.014 p.u.
Secondary Controller		
Parameters	***Symbol***	***Value***
Positive Sequence Droop Controller	m_p^+,m_I^+, n_p^+, n_I^+	*0.00005, 0.001, 0.01, 0.07*
Negative Sequence Droop Controller	m_p^-,m_I^-, n_p^-, n_I^-	*0.0005, 0.035, 0.003, 0.0006*

A lab-scale MG was also built in the laboratory [34] to validate the effectiveness of the proposed control strategy. The MG platform consists of three *Danfoss* three-phase three-leg converters with *LC* filters. Detailed electrical configuration can be seen in Fig. 6. One of the converters is utilized to emulate the grid along with a *Regatron* bidirectional DC source and extra grid impedances, while the other two converters are programmed with the proposed controller. An unbalanced load is connected between phases B and C to emulate local loads. The whole experimental test bed is shown in Fig. 22. Note that the control system is compiled to *dSPACE* system via Matlab/Simulink.

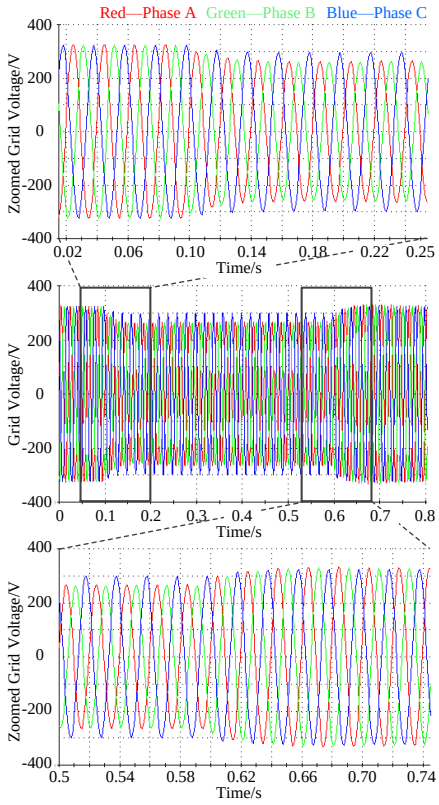

Fig. 23. Grid voltage with a two-phase 0.2 p.u. sag.

Performance of the proposed control strategy has been tested in the presence of a 0.2 p.u. two-phase voltage sag. As shown in Fig. 23, the sag occurs at t = 0.1s and clears at t = 0.6s. Based on the analysis presented in previous sections, the converter should provide positive sequence active/reactive power and negative sequence active/reactive power to compensate the voltage sag. It is worth noting that considering the converter capacity limitations, the output current is limited at 6A. Bigger inductors and higher converter capacity will contribute to restore the grid voltage, as explained in the previous sections.

As shown in Fig. 24, the active and the reactive power injected by the converters climb rapidly from 0W/Var to 1200W/Var in about 0.2s once the fault is detected. Also, it can be seen that the injected power is well shared between the two converters. Note that the value of k in (1) is set to 3 which means the power reference is 1200 W/Var. Besides, output power of the converters is set to 0 intentionally before t = 0.1s, since a power step from 0 to the required value is more challenge for the designed control system and during this period the load is energized by the grid. Fig. 25 depicts the negative sequence active and reactive power injected to the grid during the voltage sag. In the studied case, both negative sequence active and reactive power are regulated to 50W/Var due to the limitation of the converter capacity.

From Figs. 24 and 25, it is obvious that the converter can provide appropriate positive and negative sequence power according to the depth of the voltage sag. In such a way, the load voltage can be restored, and thus the customer side electrical equipment can be protected from potential damages.

To demonstrate the negative sequence voltage elimination

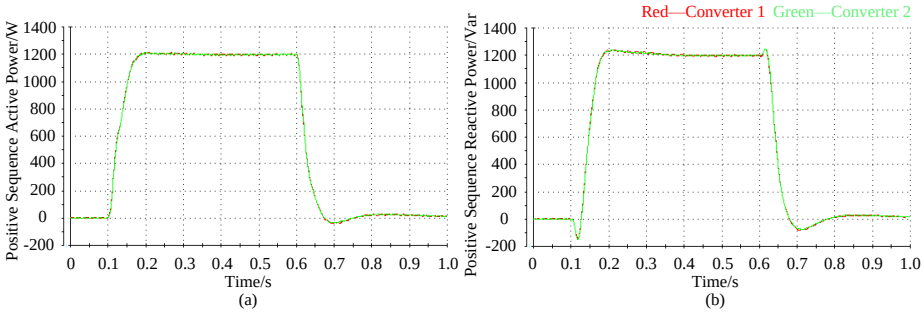

Fig. 24. Positive sequence output power of the converters. (a) active power and (b) reactive power.

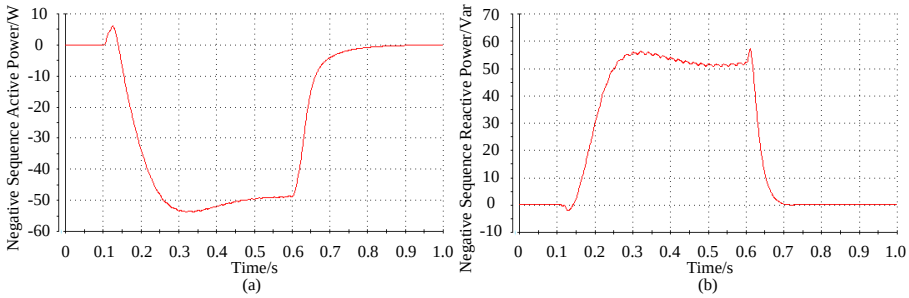

Fig. 25. Negative sequence output power of the converters. (a) active power and (b) reactive power.

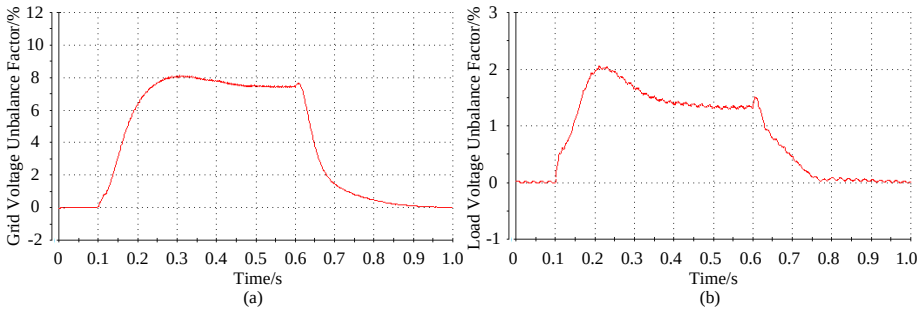

Fig. 26. Voltage unbalance factor. (a) grid voltage and (b) load voltage.

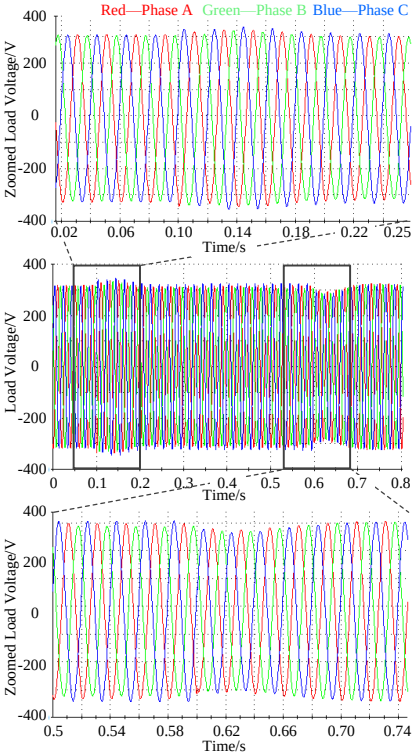

Fig. 27. Load voltage during the voltage sag.

performance, voltage unbalance factor [35], [36] of the grid voltage and load voltage are depicted in Fig. 26. As it can be seen, with the negative sequence power injection, load voltage unbalance factor decreases dramatically.

The load voltage is depicted in Fig. 27. Compared with the grid voltage shown in Fig. 23, the load voltage is boosted up and is more balanced thanks to the injected positive and negative sequence power.

In order to examine the dynamic response of the proposed LVRT controller, the converters output current waveforms are illustrated in Fig. 28. As can be seen, the current reaches the steady-state in about 5 cycles, and goes back to the pre-fault state after the sag is cleared.

In Fig. 29, phases A, B, and C output current of the converters are shown separately to examine the current sharing accuracy of the proposed control strategy. It can be seen that the current can be well shared between the converters. Note that a small difference exists in the current magnitude since the line impedances of the converters are not identical.

Moreover, since a severe grid fault (e.g. more than 2s) may occur in real applications, and under this circumstance, the MG should disconnect with the grid for safety considerations. Thus, experiments regarding transition from grid-interactive to islanded mode are performed to test the stability of the

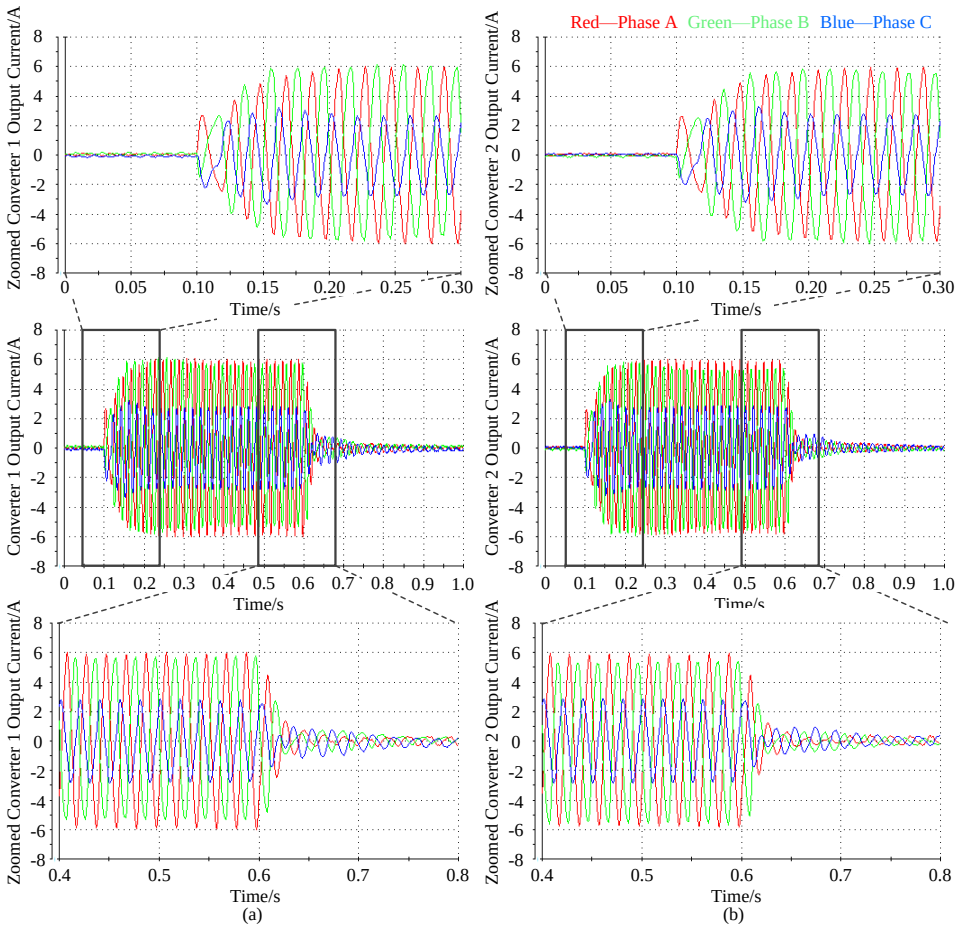

Fig. 28. Output current waveforms. (a) converter 1 and (b) converter 2.

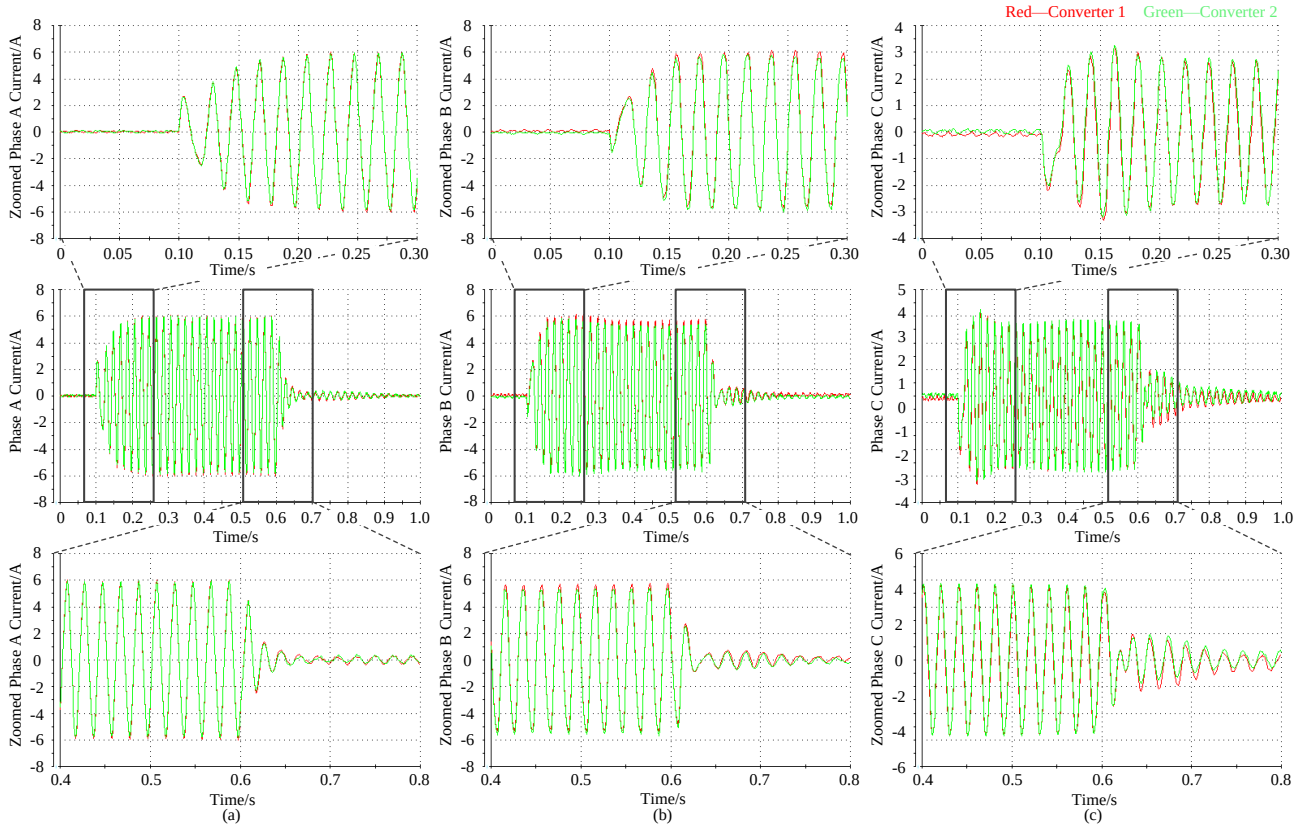

Fig. 29. Output current of converters 1 and 2. (a) phase A, (b) phase B and (c) phase C.

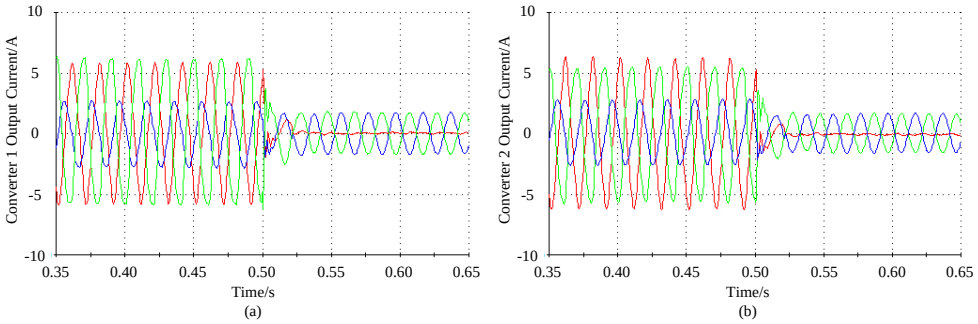

Fig. 30. Output current waveforms in transition from grid-interactive to islanded mode. (a) converter 1 and (b) converter 2.

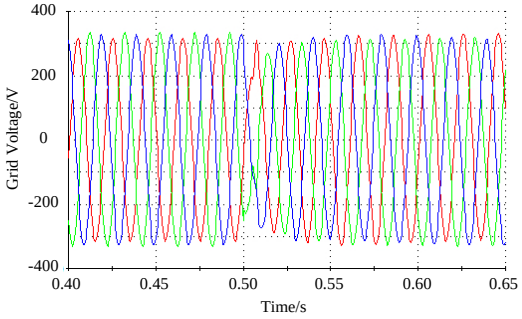

Fig. 31. Load voltage in transition from grid-interactive to islanded mode.

proposed LVRT controller. Figs. 30 and 31 show the corresponding experimental results. The disconnection of the MG occurs at t = 0.5s. As can be seen in Fig. 30, the unbalanced load can be equally shared between the converters even after disconnected with the grid. Also, the fast response allows load voltage returns to normal operation within 2 cycles, which is illustrated in Fig. 31.

VIII. Conclusion

In this paper, a negative sequence droop method based LVRT control algorithm has been proposed for grid-interactive MGs. Compared with the conventional LVRT strategies, the proposed control algorithm is capable of utilizing droop/voltage-controlled converters, which is widely used in MGs, to provide positive/negative sequence power during voltage sags. In order to explore the effect of line impedance to the system, system phasor analysis is presented under asymmetrical voltage sags. Furthermore, a power decoupling strategy is adopted to control the output power of the converter. The proposed control structure includes two levels: the primary inner loop level and secondary control level. The primary level mainly takes care of the bus voltage regulation and the current sharing among converters, while the secondary controller embeds the converter with LVRT capability. The effectiveness of the control scheme has been validated with a lab-scale MG. The obtained experimental results show that the negative and positive sequence power can be injected properly according to the grid code requirements while ensuring the current sharing accuracy among the converters.

References

[1] P. Basak, A. K. Saha, S. Chowdhury, and S. P. Chowdhury, "Microgrid: Control Techniques and Modeling," in *Proc. 44th Int. Universities Power Engineering Conf.*, 2009, pp. 1–5.

[2] A. Camacho, M. Castilla, J. Miret, R. Guzman, A. Borrell, "Reactive Power Control for Distributed Generation Power Plants to Comply With Voltage Limits During Grid Faults," *IEEE Trans. Power Electron.*, vol. 29, no. 11, pp. 6224–6234, Nov. 2014.

[3] N. Jelani, M. Molinas, "Asymmetrical Fault Ride Through as Ancillary Service by Constant Power Loads in Grid-Connected Wind Farm," *IEEE Trans. Power Electron.*, vol. 30, no. 3, pp. 1704–1713, March 2015.

[4] M. Yilmaz, P. T. Krein, "Review of the Impact of Vehicle-to-Grid Technologies on Distribution Systems and Utility Interfaces," *IEEE Trans. Power Electron.*, vol. 28, no. 12, pp. 5673–5689, Dec. 2013.

[5] N. Jelani, M. Molinas, and S. Bolognani, "Reactive Power Ancillary Service by Constant Power Loads in Distributed AC Systems," *IEEE Trans. Power Del.*, vol. 28, no. 2, pp. 920–927, Feb. 2013.

[6] A. Camacho, M. Castilla, J.Miret, J. C. Vasquez, and E. Alarcon-Gallo, "Flexible Voltage Support Control for Three-Phase Distributed Generation Inverters Under Grid Fault," *IEEE Trans. Ind. Electron.*, vol. 60, no. 4, pp. 1429–1441, Apr. 2013.

[7] M. Islam, H. Gabbar, "Study of Micro Grid Safety and Protection Strategies with Control System Infrastructures," *Smart Grid and Renewable Energy*, vol. 3, no. 1, pp. 1-9, Feb. 2012.

[8] *IEEE Standard for Interconnecting Distributed Resources with Electric Power Systems*, IEEE Standard 1547, 2003.

[9] A. Micallef, M. Apap, C. Spiteri-Staines, and J. M. Guerrero, "Single-Phase Microgrid With Seamless Transition Capabilities Between Modes of Operation," *IEEE Trans. Smart Grid*, vol. 6, no. 6, pp. 2736–2745, Nov. 2015.

[10] J. A. Laghari, H. Mokhlis, M. Karimi, A. H. A. Bakar, and H. Mohamad, "Computational Intelligence based techniques for islanding detection of distributed generation in distribution network: A review," *Energy Convers. Manage.*, vol. 88, pp. 139–152, Dec. 2014.

[11] Y. Yang, F. Blaabjerg, and Z. Zou, "Benchmarking of Grid Fault Modes in Single-Phase Grid-Connected Photovoltaic Systems," *IEEE Trans. Ind. Appl.*, vol.49, no.5, pp. 2167–2176, Sept.-Oct. 2013.

[12] X. Bao, P. Tan, F. Zhuo, and X. Yue, "Low voltage ride through control strategy for high-power grid-connected photovoltaic inverter," in Proc. *IEEE Appl. Power Electron. Conf. Expo.*, pp. 97–100, Mar. 2013.

[13] W. Guo, L. Xiao, and S, Dai, "Enhancing Low-Voltage Ride-Through Capability and Smoothing Output Power of DFIG With a Superconducting Fault-Current Limiter–Magnetic Energy Storage System," *IEEE Trans. Energy Convers.*, vol.27, no.2, pp. 277–295, June 2012.

[14] S. Hu, X. Lin, Y. Kang, and X. Zou, "An Improved Low-Voltage Ride-Through Control Strategy of Doubly Fed Induction Generator During Grid Faults," *IEEE Trans. Power Electron.*, vol. 26, no. 12, pp. 3653–3665, Dec. 2011.

[15] R. Teodorescu, M. Liserre, and P. Rodriguez, *Grid Converters for Photovoltaic and Wind Power Systems*. New York, NY, USA: IEEE-Wiley, 2011.

[16] X. Guo, X. Zhang, B. Wang, W. Wu, J. M. Guerrero, "Asymmetrical Grid Fault Ride-Through Strategy of Three-Phase Grid-Connected Inverter Considering Network Impedance Impact in Low-Voltage Grid," *IEEE Trans. Power Electron.*, vol. 29, no. 3, pp. 1064–1068, March 2014.

[17] J. C. Vasquez, R. A. Mastromauro, J. M. Guerrero, and M. Liserre, "Voltage Support Provided by a Droop-Controlled Multifunctional Inverter," *IEEE Trans. Ind. Electron.*, vol. 56, no. 11, pp. 4510–4519, Nov. 2009.

[18] J. M. Guerrero, J. Matas, L. Garc á de Vicu ña, M. Castilla, and J. Miret, "Decentralized control for parallel operation of distributed generation

inverters using resistive output impedance," *IEEE Trans. Ind. Electron*., vol. 54, no. 2, pp. 994–1004, Apr. 2007.
[19] F. Wang, J. L. Duarte, and M. A. M. Hendrix, "Pliant Active and Reactive Power Control for Grid-Interactive Converters Under Unbalanced Voltage Dips," *IEEE Trans. Power Electron*., vol. 26, no. 5, pp. 1511–1521, May 2011.
[20] Annex of O.P. 12.2. "Restricted to the technical requirements of wind power and photovoltaic facilities (Draft)," Red Electrica, [Online]. Available: http://www.ree.es.
[21] E. ON-Netz, "Grid Code - High and extra high voltage." [Online]. Available: http://www.eon-netz.com/.
[22] Energinet, "Wind Turbines Connected to Grids with Voltages below 100 kV" Regulation TF 3.2.6. [Online]. Available: http://www.energinet.dk.
[23] H. Akagi, Y. Kanazawa, and A. Nabae, "Instantaneous reactive power compensators comprising switching devices without energy storage components," *IEEE Trans. Ind. Appl*., vol. 20, no. 3, pp. 625–630, May 1984.
[24] W. Yao, M. Chen; J. Matas, J. M. Guerrero, Z. Qian, "Design and Analysis of the Droop Control Method for Parallel Inverters Considering the Impact of the Complex Impedance on the Power Sharing," *IEEE Trans. Ind. Electron*., vol. 58, no. 2, pp. 576–588, Feb. 2011.
[25] U. Borup, F. Blaabjerg, and P. N. Enjeti, "Sharing of nonlinear load in parallel-connected three-phase converters," *IEEE Trans. Ind. Appl*., vol. 37, no. 6, pp. 1817–1823, Nov./Dec. 2001.
[26] L. Corradini, P. Mattavelli, M. Corradin, F. Polo, "Analysis of Parallel Operation of Uninterruptible Power Supplies Loaded Through Long Wiring Cables," *IEEE Trans. Power Electron*., vol. 25, no. 4, pp. 1046–1054, Apr. 2010.
[27] J. M. Guerrero, M. Chandorkar, T. Lee, P. C. Loh, "Advanced Control Architectures for Intelligent Microgrids—Part I: Decentralized and Hierarchical Control," *IEEE Trans. Ind. Electron*., vol. 60, no.4, pp.1254–1262, April 2013.
[28] J. M. Guerrero, J. C. Vasquez, J. Matas, L. G. de Vicuna, and M. Castilla, "Hierarchical control of droop-controlled AC and DC microgrids—A general approach towards standardization," *IEEE Trans. Ind. Electron*., vol. 58, no. 1, pp. 158–172, Jan. 2011.
[29] J. M. Guerrero, J. Matas, L. G. de Vicuña, M. Castilla, and J. Miret, "Wireless-Control Strategy for Parallel Operation of Distributed-Generation Inverters," *IEEE Trans. Ind. Electron*., vol. 53, no. 5, pp. 1461–1470, Oct. 2006.
[30] D. N. Zmood and D. G. Holmes, "Stationary frame current regulation of PWM inverters with zero steady-state error," *IEEE Trans. Power Electron*., vol. 18, no. 3, pp. 814–822, May 2003.
[31] J. C. Vasquez, J. M. Guerrero, M. Savaghebi, J. Eloy-Garcia, and R. Teodorescu, "Modeling, analysis, and design of stationary-reference-frame droop-controlled parallel three-phase voltage source inverters," *IEEE Trans. Ind. Electron*., vol. 60, no. 4, pp. 1271–1280, April 2013.
[32] P. Rodriguez, A. Luna, I. Etxeberria, J. R. Hermoso and R. Teodorescu, "Multiple second order generalized integrators for harmonic synchronization of power converters," in Proc. *IEEE Energy Convers. Congress Expo*., pp. 2239–2246, Sep. 2009.
[33] M. H. Bollen, Understanding power quality problem: voltage sags and interruptions. Piscataway, NJ, USA: IEEE Press, Oct. 1999.
[34] Microgrid Research Programme. URL: www.microgrids.et.aau.dk.
[35] R. C. Dugan, M. F. McGranaghan, S. Santoso, and H. W. Beaty, Electrical Power Systems Quality. New York, NY, USA: McGraw-Hill, Jan. 2012.
[36] L. Meng, X. Zhao, F. Tang, M. Savaghebi, T. Dragicevic, J. Vasquez, J. Guerrero, "Distributed Voltage Unbalance Compensation in Islanded Microgrids by Using Dynamic-Consensus-Algorithm," *IEEE Trans. Power Electron*., vol. 31, no. 1, pp. 827–838, Jan. 2016.

Xin Zhao (S'15) received the B.S. and M.S. degrees in Power Electronics & Electrical Drives from Northwestern Polytechnical University, Xi'an, China, in 2010 and 2013, respectively. He is currently pursuing the Ph.D. degree at the Department of Energy Technology, Aalborg University, Denmark.

His research interests include microgrids, distributed generation systems, control of power converters, and power quality issues in microgrids.

Josep M. Guerrero (S'01-M'04-SM'08-FM'15) received the B.S. degree in telecommunications engineering, the M.S. degree in electronics engineering, and the Ph.D. degree in power electronics from the Technical University of Catalonia, Barcelona, in 1997, 2000 and 2003, respectively. Since 2011, he has been a Full Professor with the Department of Energy Technology, Aalborg University, Denmark, where he is responsible for the Microgrid Research Program. From 2012 he is a guest Professor at the Chinese Academy of Science and the Nanjing University of Aeronautics and Astronautics; from 2014 he is chair Professor in Shandong University; from 2015 he is a distinguished guest Professor in Hunan University; and from 2016 he is a visiting professor fellow at Aston University, UK.

His research interests is oriented to different microgrid aspects, including power electronics, distributed energy-storage systems, hierarchical and cooperative control, energy management systems, smart metering and the internet of things for AC/DC microgrid clusters and islanded minigrids; recently specially focused on maritime microgrids for electrical ships, vessels, ferries and seaports. Prof. Guerrero is an Associate Editor for the IEEE TRANSACTIONS ON POWER ELECTRONICS, the IEEE TRANSACTIONS ON INDUSTRIAL ELECTRONICS, and the IEEE Industrial Electronics Magazine, and an Editor for the IEEE TRANSACTIONS on SMART GRID and IEEE TRANSACTIONS on ENERGY CONVERSION. He has been Guest Editor of the IEEE TRANSACTIONS ON POWER ELECTRONICS Special Issues: Power Electronics for Wind Energy Conversion and Power Electronics for Microgrids; the IEEE TRANSACTIONS ON INDUSTRIAL ELECTRONICS Special Sections: Uninterruptible Power Supplies systems, Renewable Energy Systems, Distributed Generation and Microgrids, and Industrial Applications and Implementation Issues of the Kalman Filter; the IEEE TRANSACTIONS on SMART GRID Special Issues: Smart DC Distribution Systems and Power Quality in Smart Grids; the IEEE TRANSACTIONS on ENERGY CONVERSION Special Issue on Energy Conversion in Next-generation Electric Ships. He was the chair of the Renewable Energy Systems Technical Committee of the IEEE Industrial Electronics Society. He received the best paper award of the IEEE Transactions on Energy Conversion for the period 2014-2015. In 2014 and 2015 he was awarded by Thomson Reuters as Highly Cited Researcher, and in 2015 he was elevated as IEEE Fellow for his contributions on "distributed power systems and microgrids."

Mehdi Savaghebi (S'06-M'15-SM'15) was born in Karaj, Iran, in 1983. He received the B.Sc. degree from University of Tehran, Iran, in 2004 and the M.Sc. and Ph.D. degrees with highest honors from Iran University of Science and Technology, Tehran, Iran in 2006 and 2012, respectively, all in Electrical Engineering. From 2007 to 2014, he was a Lecturer in Electrical Engineering Department, Karaj Branch, Azad University where he taught various courses and conducted research on power systems and electrical machines. In 2010, he was a Visiting Ph.D. Student with the Department of Energy Technology, Aalborg University, Aalborg, Denmark and with the Department of Automatic Control Systems and Computer Engineering, Technical University of Catalonia, Barcelona, Spain.

Currently, he is a Postdoctoral Fellow in Department of Energy Technology, Aalborg University. His main research interests include distributed generation systems, microgrids, power quality and smart metering. Dr. Savaghebi is a member of Technical Committee of Renewable Energy Systems, IEEE Industrial Electronics Society and also IEEE Task Force on Microgrids Stability Analysis and Modeling.

Juan C. Vasquez (M'12-SM'14) received the B.S. degree in electronics engineering from the Autonomous University of Manizales, Manizales, Colombia, and the Ph.D. degree in automatic control, robotics, and computer vision from the Technical University of Catalonia, Barcelona, Spain, in 2004 and 2009, respectively. He was with the Autonomous University of Manizales working as a teaching assistant and the Technical University of Catalonia as a Post-Doctoral Assistant in 2005 and 2008 respectively. In 2011, he was Assistant Professor and from 2014 he is working as an Associate Professor at the Department of Energy Technology, Aalborg University, Denmark where he is the Vice Programme Leader of the Microgrids Research Program. From Feb. 2015 to April. 2015 he was a Visiting Scholar at the Center of Power Electronics Systems (CPES) at Virginia Tech. His current research interests include operation, advanced hierarchical and cooperative control, optimization and energy management applied to distributed generation in AC and DC microgrids. He has authored and co-authored more than 100 technical papers only in Microgrids in international IEEE conferences and journals.

Dr. Vasquez is currently a member of the IEC System Evaluation Group SEG4 on LVDC Distribution and Safety for use in Developed and Developing Economies, the Renewable Energy Systems Technical Committee TC-RES in IEEE Industrial Electronics, PELS, IAS, and PES Societies.

Xiaohua Wu received the B.E., M.E., and Ph.D. degrees in electrical engineering from Northwestern Polytechnical University, Xi'an, China, in 1992, 1994, and 2004, respectively. She joined the faculty of Automation, Northwestern Polytechnical University, in 1994, where she is currently a Professor.

Her current research interests include control of power converters, distributed generation systems, power quality issues in microgrids, and modeling of power electronic devices.

Kai Sun (M'12-SM'16) received the B.E., M.E., and Ph.D. degrees in electrical engineering from Tsinghua University, Beijing, China, in 2000, 2002, and 2006, respectively.

He joined the faculty of Electrical Engineering, Tsinghua University, in 2006, where he is currently an Associate Professor. From 2009 to 2010, he was a Visiting Scholar of Electrical Engineering with the Institute of Energy Technology, Aalborg University, Aalborg, Denmark. His current research interests include power electronics for renewable generation systems, microgrids, and active distribution networks.

Dr. Sun is a member of IEEE Industrial Electronics Society Renewable Energy Systems Technical Committee, a member of IEEE Power Electronics Society Technical Committee of Sustainable Energy Systems, and a member of Awards Sub-committee of IEEE Industry Application Society Industrial Drive Committee. He is an Associate Editor for the Journal of POWER ELECTRONICS. He was a recipient of the Delta Young Scholar Award in 2013.